Naval Research Laboratory

Washington, DC 20375-5320

NRL/5650/MR--2021/1

An Overview of Techniques for Combining RF-Modulated Optical Signals

Frank Bucholtz

Jacobs, Inc.
Dallas, Texas

Christopher S. McDermitt

J.M. Singley

Photonics Technology Branch
Optical Sciences Division

January 28, 2021

REPORT DOCUMENTATION PAGE

Form Approved
OMB No. 0704-0188

1. REPORT DATE *(DD-MM-YYYY)*	**2. REPORT TYPE**	**3. DATES COVERED** *(From - To)*
28-01-2021	NRL Memorandum Report	1 Jan 2016 – 30 Dec 2019

4. TITLE AND SUBTITLE

An Overview of Techniques for Combining RF-Modulated Optical Signals

5a. CONTRACT NUMBER

5b. GRANT NUMBER

5c. PROGRAM ELEMENT NUMBER
62271N

6. AUTHOR(S)

Frank Bucholtz*, Christopher S. McDermitt, and J. M. Singley

5d. PROJECT NUMBER

5e. TASK NUMBER
EW-271-012

5f. WORK UNIT NUMBER
6B50

7. PERFORMING ORGANIZATION NAME(S) AND ADDRESS(ES)

Naval Research Laboratory
4555 Overlook Avenue, SW
Washington, DC 20375-5320

8. PERFORMING ORGANIZATION REPORT NUMBER

NRL/5650/MR--2021/1

9. SPONSORING / MONITORING AGENCY NAME(S) AND ADDRESS(ES)

Office of Naval Research
One Liberty Center
875 North Randolph Street
Arlington, VA 22203-1995

10. SPONSOR / MONITOR'S ACRONYM(S)

ONR

11. SPONSOR / MONITOR'S REPORT NUMBER(S)

12. DISTRIBUTION / AVAILABILITY STATEMENT

DISTRIBUTION STATEMENT A: Approved for public release; distribution is unlimited.

13. SUPPLEMENTARY NOTES

* Jacobs, Inc., 1999 Bryan Street, Suite 1200, Dallas, Texas 75201

14. ABSTRACT

In this report we analyze a number of architectures for combining RF-modulated optical signals in terms of susceptibility to optical interference.

15. SUBJECT TERMS

Photonics
Analog photonics
Microwave photonics
Optical interference
RF signal processing

16. SECURITY CLASSIFICATION OF:			**17. LIMITATION OF ABSTRACT**	**18. NUMBER OF PAGES**	**19a. NAME OF RESPONSIBLE PERSON**
a. REPORT	**b. ABSTRACT**	**c. THIS PAGE**			Joseph M. Singley
Unclassified Unlimited	Unclassified Unlimited	Unclassified Unlimited	Unclassified Unlimited	33	**19b. TELEPHONE NUMBER** *(include area code)* (202) 404-1012

This page intentionally left blank.

Contents

This page intentionally left blank.

1 EXECUTIVE SUMMARY

Processing RF signals in the optical domain offers a host of advantages over RF-domain processing, the most prominent being large true-time delay accompanied with small RF loss even at high RF frequencies. In applications such as filtering and beamforming it is necessary to combine a number of RF-modulated optical signals to produce a single RF output. However, the advantages of the optical domain processing come with the potential for RF instability due to coherent optical effects. In this report we analyze a number of architectures for combining RF-modulated optical signals in terms of susceptibility to optical interference.

This report is based on one in a series of lectures presented by F. Bucholtz to the Optical Sciences Division, NRL, during the three-year period 2016-2019.

This page intentionally left blank.

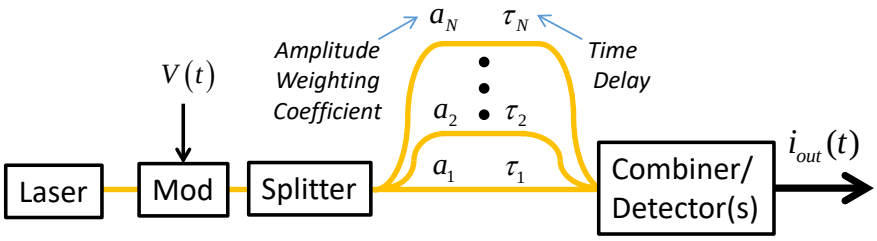

Figure 1: A finite-impulse-response (FIR) filter implemented using optical fibers. Mod = device to modulate the RF signal $V(t)$ onto the optical carrier provided by the laser. a_n and τ_n are amplitude weighting coefficients and relative time delays, respectively. The output photocurrent is labelled $i_{out}(t)$.

2 Introduction

The world of digital communications is pushing to ever-higher RF frequencies where intrinsic losses make it infeasible to accomplish such tasks as signal transmission and signal processing entirely in the RF domain, that is, in copper cable. Those tasks can now be accomplished largely in the optical domain, especially by systems utilizing single-mode fiber with a spectrally-pure optical carrier provided by a laser diode [1, 2, 3]. Using a modulating device, an optical carrier is mixed with an RF signal which is then transmitted and processed as an optical sideband, enjoying all the benefits of life in the optical domain. But the spectral purity of the light brings with it the danger of coherent optical effects – optical interference – arising from very small changes in optical length due to changes in temperature or strain of the fibers in the system. Whereas a length change in an RF cable of 2.5 mm is required to cause a 180 deg phase shift at 40 GHz, a length change of only 0.75 µm in optical fiber causes a 180 deg phase shift at 1500 nm. The environmental perturbations responsible for these shifts are typically time-dependent and can produce unwanted amplitude and phase variations in the recovered RF signal. Hence, care must be taken in system design and operation to mitigate the effects of optical coherence.

A common signal processing system is the finite-impulse-response (FIR) filter shown in Fig. 1, also referred to as a moving average (MA) filter [4]. The filter input is an RF voltage $V(t)$ and each of the N taps is characterized by an amplitude weighting coefficient a_n and a time delay τ_n. The desired output photocurrent is a linear sum of weighted, time-delayed versions of the input voltage

Manuscript approved January 19, 2021.

$$i_{out}(t) = \sum_{n=1}^{N} a_n V(t - \tau_n). \tag{1}$$

In the optical domain, the challenge is to implement the box labelled "Combiner/Detector(s)" so that the output is indeed just Eq. (1) with no additional, unwanted fluctuating terms.

In the following we will examine four different approaches for combining RF-modulated, optical-domain signals. We will use the FIR filter as a standard system for comparing the susceptibility of various combination techniques to optical interference. With one exception, the analysis will be performed using only scalar fields, that is, neglecting polarization effects. The analysis will not consider dispersion, multi-tone effects due to nonlinearities, or noise performance.

Before proceeding we first develop some background material comprising a) a summary of matrices useful for the analysis of two-tap systems, and b) a quick review of the nature of optical interference.

3 Background

3.1 Matrices for Lossless 4-port Devices

In Fig. 2 we present a set of 2×2 matrix tools that will streamline the subsequent analysis. Each matrix represents the forward scattering matrix for the scalar electric fields for an optical 4-port device, that is, an optical device comprising two input ports and two output ports. In each case, the input fields E_1 and E_2 are transformed by the device to produce output fields E_3 and E_4 according to

$$\begin{bmatrix} E_3 \\ E_4 \end{bmatrix} = \mathbf{M} \begin{bmatrix} E_1 \\ E_2 \end{bmatrix}. \tag{2}$$

where $\mathbf{M}$ is a 2×2 matrix with complex elements. In assuming the device is lossless, the matrix must be unitary, that is, $\mathbf{M}$ must satisfy $\mathbf{M}^{-1}\mathbf{M}^{\dagger} = \mathbf{M}^{\dagger}\mathbf{M}^{-1} = \mathbf{I}$ and $|\det \mathbf{M}| = 1$ and where $\dagger$ indicates Hermitian adjoint (conjugate transpose), $\mathbf{I}$ is the identity matrix and *det* signifies determinant. (Note: In order to avoid confusion at this point, we note explicitly that the matrices in Fig. 2 are *not* Jones matrices for polarization states, they are transformation matrices for scalar fields. Jones matrices describe the transformation of two orthogonal polarization states in a single waveguide (or in a single mode) while the matrices here describe the transformation of scalar fields in two spatially-distinct waveguides.) Although we

a) Lossless, symmetric 50:50 coupler w/no reflections. (det = 1 imposed)

$$M = \frac{1}{\sqrt{2}}\begin{bmatrix} 1 & j \\ j & 1 \end{bmatrix}$$

b) Lossless, $\alpha^2 : (1-\alpha^2)$ coupler w/no reflections. (det = 1 imposed)

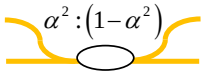

$$\begin{bmatrix} \alpha & j\sqrt{1-\alpha^2} \\ j\sqrt{1-\alpha^2} & \alpha \end{bmatrix}$$

c) Lossless, relative delay where operator $\Gamma(\tau)$ delays the time in any function to the right by $\tau : \Gamma(\tau)g(t) = g(t-\tau)$.

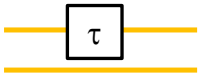

$$\begin{bmatrix} \Gamma(t) & 0 \\ 0 & 1 \end{bmatrix}$$

d) Lossless optical phase shifter.

$$\begin{bmatrix} \exp(j\phi) & 0 \\ 0 & 1 \end{bmatrix}$$

e) Lossless amplitude modulator. (balanced, chirp-free)

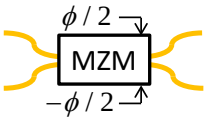

$$j\begin{bmatrix} \sin(\phi/2) & \cos(\phi/2) \\ \cos(\phi/2) & -\sin(\phi/2) \end{bmatrix}$$

f) Lossless amplitude modulator. (unbalanced)

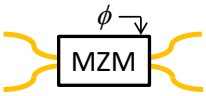

$$\frac{1}{2}\begin{bmatrix} \exp(j\phi)-1 & j(\exp(j\phi)+1) \\ j(\exp(j\phi)+1) & -(\exp(j\phi)-1) \end{bmatrix}$$
$$= je^{j\phi/2}\begin{bmatrix} \sin(\phi/2) & \cos(\phi/2) \\ \cos(\phi/2) & -\sin(\phi/2) \end{bmatrix}$$

Figure 2: Summary of matrix representations for various lossless optical 4-port devices.

presented time delay and phase shift as distinct operations in Fig. 2 (c) and (d), respectively, phase shift is really just a specific case of the more general time-delay operator $\Gamma(\tau)$ defined by $\Gamma(\tau)f(t) = f(t-\tau)$ for any function of time $f(t)$. If the field incident on port 1 is purely monochromatic with optical radian frequency ω and fixed phase ϕ_0, $E_1(t) = E_0 \exp(j\omega t)\exp(j\phi_0)$, then the time-delay operator produces simply a phase shift,

$$\begin{aligned} \Gamma(\tau)E_1(t) &= E_0 \exp(j\omega(t-\tau))\exp(j\phi_0) \\ &= E_0 \exp(j\omega t)\exp(j\phi_0)\exp(j\phi) \end{aligned} \tag{3}$$

where $\phi = \omega\tau$. On the other hand, if the amplitude and/or the phase of the incident field is time dependent then the time delay operator *must* be used since the result is then not simply a phase shift:

$$\Gamma(\tau)E_1(t) = E_0(t-\tau)\exp(j\omega(t-\tau))\exp(j\phi_0(t-\tau)). \tag{4}$$

As a practical matter, you can usually get away with just a phase shift even when the incoming field is modulated provided the modulation frequency is much less than $1/\tau$.

3.2 Review of the Single-Channel, IM-DD RF Photonic Link

In this section we review very briefly the relationship between the input RF voltage and the output photocurrent in what is commonly referred to as an IM-DD link (intensity-modulated, direct-detection) – a system for transporting RF signals in the optical domain [1]. The simple implementation of an IM-DD link shown in Fig. 3 comprises a laser source, a Mach-Zehnder modulator (MZM), and a photodetector (PD). The input voltage to the MZM is the sum of two terms, a DC voltage V_{dc} and an RF voltage $v_0 sin\Omega t$ at RF frequency $f_{rf} = \Omega/2\pi$.

In simple terms, the RF voltage applied to the MZM modulates the intensity of the optical carrier provided by the laser operating at optical frequency ω. In the limit of small modulation depth, and for the proper choice of V_{dc}, the optical electric field at the MZM output consists of three terms: the optical carrier at frequency ω, and two in-phase sidebands at frequencies $\omega \pm \Omega$,

$$E_{MZM} = E_c(\omega) + E_s(\omega+\Omega) + E_s(\omega-\Omega) \tag{5}$$

and where the sideband amplitudes are proportional to v_0. The optical power at the PD input and, correspondingly, the photocurrent i_{out} at the PD output, are proportional to $|E_{MZM}|^2$ thus resulting in a term in $i_{out}(t)$ that

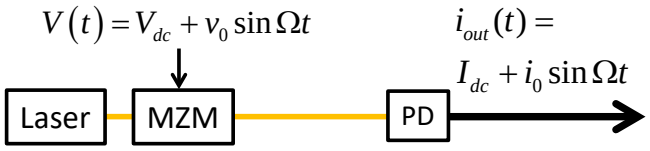

Figure 3: A simple, analog IM-DD (intensity-modulated, direct-detection) photonic link. MZM = Mach-Zehnder (intensity) modulator, PD = photodetector.

is proportional to the input RF voltage $v_0 \sin \Omega t$. The RF signal has thus propagated in the optical domain and has been recovered in the electrical domain as an RF current at the PD output.

3.3 Comparison to the RF Scattering Matrix

It is natural to ask about the relationship, if any, between the scattering-matrices given above for 4-port optical devices and the traditional RF scattering matrix measured by a network analyzer and that gives rise, for example, to the parameter $S21$. The difference is simple. Whereas the optical scattering matrix only accounts for signals entering ports 1 and 2 and exiting ports 3 and 4, the RF scattering matrix assumes the presence of signals both into and out of each port. As a result, while a 2×2 matrix is typically sufficient to represent a 4-port optical device, a 4-port RF device would require a 4×4 matrix.

Following Pozar [5], let v_n^+ represent the RF voltage entering port n and let v_n^- represent the RF voltage exiting port n. (Note: Some texts use the language "incident on port n" and "reflected from port n" but this can be misleading since the word "reflected" sometimes refers to an unwanted effect.) Then, for a 2-port RF device, such as an amplifier or attenuator,

$$\begin{bmatrix} v_1^- \\ v_2^- \end{bmatrix} = \begin{bmatrix} S_{11} & S_{12} \\ S_{21} & S_{22} \end{bmatrix} \begin{bmatrix} v_1^+ \\ v_2^+ \end{bmatrix} \tag{6}$$

while for a 4-port RF device, such as a 2×2 splitter or combiner,

$$\begin{bmatrix} v_1^- \\ v_2^- \\ v_3^- \\ v_4^- \end{bmatrix} = \begin{bmatrix} S_{11} & S_{12} & S_{13} & S_{14} \\ S_{21} & S_{22} & S_{23} & S_{24} \\ S_{31} & S_{32} & S_{33} & S_{34} \\ S_{41} & S_{42} & S_{43} & S_{44} \end{bmatrix} \begin{bmatrix} v_1^+ \\ v_2^+ \\ v_3^+ \\ v_4^+ \end{bmatrix}. \tag{7}$$

If we allow only two input signals v_1^+ and v_2^+ and only two output signals v_3^- and v_4^- in Eq. (7), then the operation of a 4-port RF device can indeed be

represented completely by just the 2×2 submatrix in the lower left corner of the full 4×4 matrix

$$\begin{bmatrix} v_3^- \\ v_4^- \end{bmatrix} = \begin{bmatrix} S_{31} & S_{32} \\ S_{41} & S_{42} \end{bmatrix} \begin{bmatrix} v_1^+ \\ v_2^+ \end{bmatrix}, \tag{8}$$

a description that is equivalent to the optical scattering matrices in Fig. 2.

3.4 Review of the Nature of Interference

Since we will be interested in the possible deleterious effects of optical coherence it will be useful to review briefly the origins of optical interference. Consider two scalar fields E_1 and E_2 that are monochromatic at the same optical frequency and incident simultaneously on a photodetector. Write the amplitude and phase of each field as $E_{1,2} = E_{01,02} \exp(j\phi_{1,2})$. Then the total field at the PD is just $E_{PD} = E_1 + E_2$ and the photocurrent i_{PD} is proportional to the optical power,

$$i_{PD} \propto |E_{PD}|^2 = |E_1 + E_2|^2 = E_{01}^2 + E_{02}^2 + 2E_{01}E_{02}\cos(\phi_2 - \phi_1). \tag{9}$$

The last term is the interference where $\cos(\phi_2 - \phi_1)$ can vary between ± 1 as the phase difference $(\phi_2 - \phi_1)$ varies over $[0, 2\pi)$.

The alert reader has noticed a serious problem with Eq. (9), namely, optical power has not been conserved! We started with power $E_{01}^2 + E_{02}^2$ and we ended up with power somewhere in the range $E_{01}^2 + E_{01}^2 \pm 2E_{01}E_{02}$. The problem arises with the seemingly innocent assumption we made above that the two fields were "... incident simultaneously on a photodetector." How, exactly, did that happen? There are two possibilities as shown in Fig. 4. In the first approach, shown in Fig. 4(a), the fields arrive at the PD from different angles (different $\hat{k}$ vectors); in the second approach, shown in Fig. 4(b), the two fields were aligned to a common $\hat{k}$ vector using a beamsplitter or coupler.

We first analyze the second approach using the matrix representation in Fig. 2(a). Then

$$\begin{bmatrix} E_3 \\ E_4 \end{bmatrix} = \frac{1}{\sqrt{2}} \begin{bmatrix} 1 & j \\ j & 1 \end{bmatrix} \begin{bmatrix} E_1 \\ E_2 \end{bmatrix} = \frac{1}{\sqrt{2}} \begin{bmatrix} E_1 + jE_2 \\ jE_1 + E_2 \end{bmatrix} \tag{10}$$

and the optical powers at the output ports of the beamsplitter are given by

$$\begin{bmatrix} p_3 \\ p_4 \end{bmatrix} \propto \begin{bmatrix} |E_3|^2 \\ |E_4|^2 \end{bmatrix} = \frac{1}{2} \begin{bmatrix} E_{01}^2 + E_{02}^2 + 2E_{01}E_{02}\sin(\phi_2 - \phi 1) \\ E_{01}^2 + E_{02}^2 - 2E_{01}E_{02}\sin(\phi_2 - \phi 1) \end{bmatrix}. \tag{11}$$

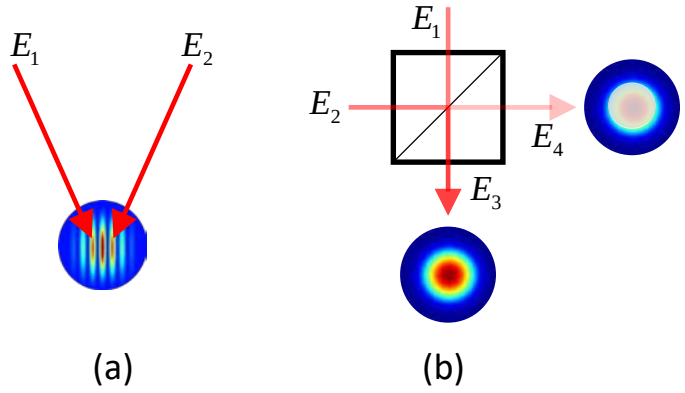

Figure 4: Two approaches for combining two beams on a photodetector.

We see now that total power is conserved since $p_3+p_4 = E_{01}^2+E_{02}^2 = p_1+p_2$ and we see further that, as the phase difference $(\phi_2-\phi_1)$ is varied, any power removed from port 3 must appear at port 4 and vice versa.

Returning now to the first approach, seen in Fig. 4(a), we will not go through the details of the analysis of the interference pattern but it can be found in many textbooks [6, 7, 8] as it is equivalent to a double-pinhole (double-slit) experiment. Shown in the figure is an example of the resultant spatial interference pattern, comprising areas of high and low intensity, that forms on the photodetector . As the phase difference $(\phi_2 - \phi_1)$ is varied, the interference pattern shifts back and forth but the total optical power contained in the entire interference pattern remains fixed.

An important property of an interferometer is the so-called **fringe visibility**, denoted by γ, which is a measure of the strength of the interference term compared to the non-interferometric (DC) portion of the optical power. Fringe visibility is summarized in Fig. 5.

In RF photonics we employ exclusively continuous-wave or pulsed optical signals containing a large number of photons and we are thus usually justified in using scalar, classical fields for system analysis. (An exception is when we exploit the polarization properties of light, discussed below in the context of a multiplexing approach, in which case the full vector field must be used.) Given N classical, scalar fields $E_1, E_2, \cdots, E_N$ incident simultaneously on a photodetector the output photocurrent is proportional to $|E_1+E_2+\cdots+E_N|^2$ which gives rise to two types of output terms. The first

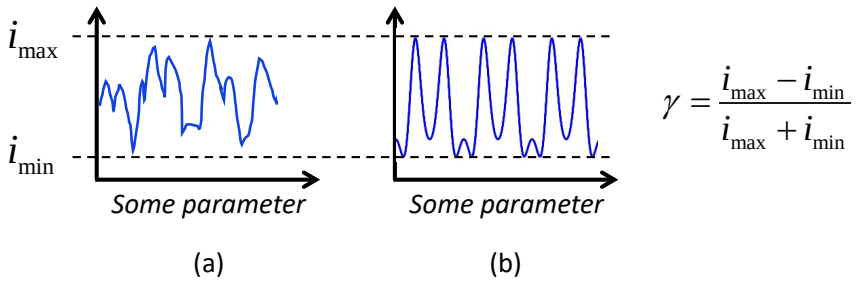

Figure 5: The plot shows output photocurrent as a function of time under the variation of some parameter such as phase difference or wavelength. (a) random variation of the parameter, and (b) large-amplitude sinusoidal variation of the parameter. The fringe visibility γ is defined in the inset.

type are of the form $|E_n|^2$ where each field interacts with itself to produce DC photocurrent. The second type are interference terms between different fields $E_n E_m^*$ $(n \neq m)$. The mental picture we have for classical fields then is one in which interference arises when two or more coherent fields overlap in time and space at the photodetector. But there is another view of the origin of interference.

In the field of quantum optics, interference experiments have been conducted in which only one photon at a time is injected into an interferometer such as the two-slit set-up shown in Fig. 6. A succession of single photons is sent to the slits and the position at which the photon strikes the screen is recorded. After a large number of single photons have been sent through the apparatus, a spatial interference pattern emerges in the recorded positions of photons on the screen. Holding the view that the photon is a particle, each photon went through either one slit or the other and, yet, the resultant built-up interference pattern suggests each photon "knew" about the other slit and behaved just like a classical wave. More complex and sophisticated versions of this this single photon interferometer have been conducted and are reported under descriptors such as welcher-weg (which-way) experiments [11], delayed-choice experiments [12], and quantum eraser experiments [12]. One significant outcome of these experiments is a viewpoint in which the potential for interference is present whenever there is uncertainty about which photon took which path through an apparatus. It is this uncertainty itself that gives rise to optical interference, without the need for two or more fields to be present simultaneously at a detector. Said another way, if a photon has

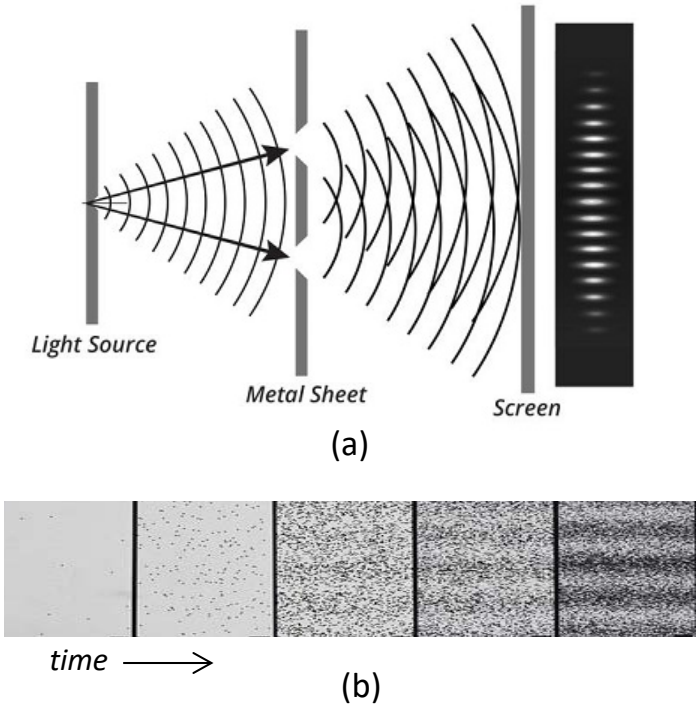

Figure 6: The classic two-slit (double-slit) optical interferometer. (a) Experimental arrangement comprising light from a single source incident on an opaque sheet with two openings and a photodetection screen. The resultant interference pattern for classical light is shown [9]. (b) Result of the same experiment as in (a) but where only one photon at a time was incident on the metal sheet containing the slits. Over time, the exact same interference pattern forms [10]

.

travel options in reaching a photodetector and its exact route isn't known, then interference effects are possible. For a good popular account of these topics see, for example, Ananthaswamy [13].

Suppose we define a "certainty" factor K, such that

$$\begin{cases} K = 1 & \text{photon and path are known with complete certainty,} \\ 0 < K < 1 & \text{photon and path known only partially,} \\ K = 0 & \text{photon and path are completely uncertain.} \end{cases} \tag{12}$$

Then the fringe visibility γ and K are related by [14]

$$\gamma^2 + K^2 = 1. \tag{13}$$

For single-photon experiments K can often be defined quantitatively in terms of system parameters and the input state of light but, for classical, fields, Eq. (13) is more of a qualitative reminder that there exists a fundamental trade-off between interferometric fringe visibility and knowledge of which one of the available alternate paths was actually taken by a particular photon. In an FIR filter, the alternate paths are quite obvious – they are the N individual delay lines.

In the discussion to follow, we will be careful to use language in which we say that a high degree of path uncertainty leads to the "potential for interference" or "can exhibit optical interference" rather than stating unequivocally that uncertainty leads to interference. The reason is that the interferometric fringe visibility depends in practice, not only on uncertainty, but also on additional factors such as temporal and spatial coherence properties of the source and polarization effects – a full discussion of which is beyond the scope of this report. So, even if the uncertainty is high, interference may not be observed due to other mitigating factors.

That concludes the brief review of interference. In the next section we analyze five approaches for combining the signals from N delay lines in an FIR filter implemented in the optical domain.

4 Signal Combination Approaches

We now discuss four feasible architectures for implementing an FIR structure in the optical domain summarized in Fig. 7. They are

A) Photodetect the light directly from each path and combine in the RF domain;

B) combine light from each path in the optical domain using a fiber coupler and photodetect any one coupler output;

C) combine the light from each path directly at the photodetector using a fiber bundle; and

D) multiplex each path onto a single fiber in the optical domain using a standard multiplexing scheme.

To simplify the analysis we will consider only a two-tap version of each approach but that will be sufficient to evaluate the susceptibility of the approach to coherent optical effects.

Before getting to the full analysis we first analyze the two-beam structure shown in Fig. 8 since this partial system forms the basis for all the approaches. The E-fields at various locations in the system are labelled in

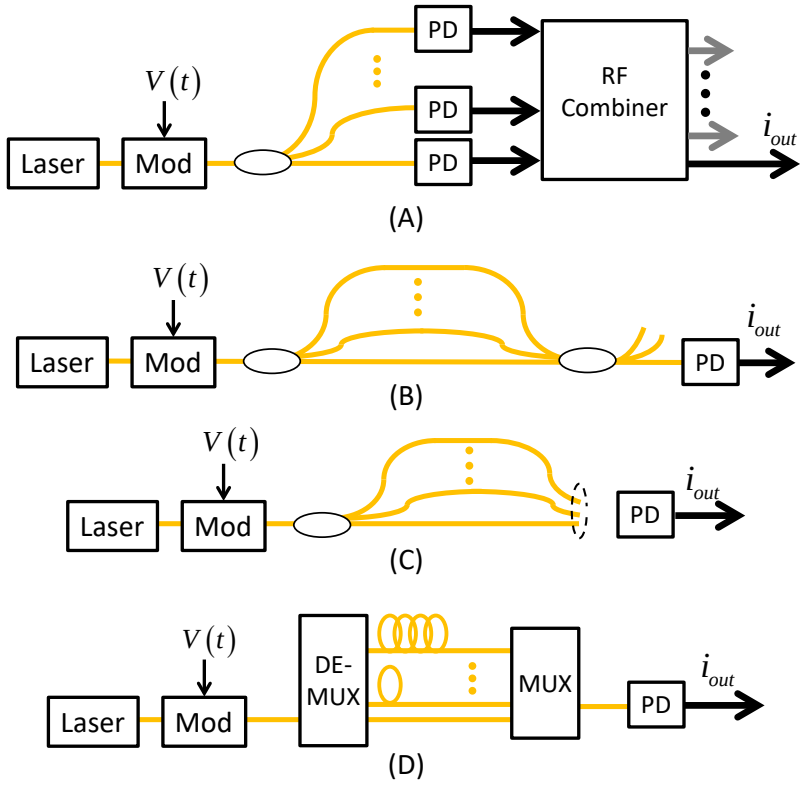

Figure 7: Four feasible approaches for implementing an RF finite-impulse response (FIR) filter in the optical domain.

the figure and the analysis proceeds by simple matrix multiplication using the appropriate matrices from Fig. 2.

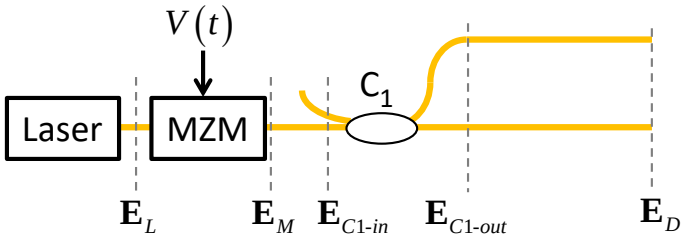

Figure 8: Partial system.

Write the field at the laser output as

$$\mathbf{E}_L = E_0 \exp(j\omega t) \begin{bmatrix} 1 \\ 0 \end{bmatrix} \equiv E(t) \begin{bmatrix} 1 \\ 0 \end{bmatrix}. \tag{14}$$

where $\omega = 2\pi\nu$ for optical frequency ν. Next, assume the MZM is a chirp-free device and use the matrix in Fig. 2(e) to write the MZM output as

$$\mathbf{E}_M = j \begin{bmatrix} \sin(\phi/2) & \cos(\phi/2) \\ \cos(\phi/2) & -\sin(\phi/2) \end{bmatrix} \left(E(t) \begin{bmatrix} 1 \\ 0 \end{bmatrix} \right) = jE(t) \begin{bmatrix} \sin(\phi/2) \\ \cos(\phi/2) \end{bmatrix} \tag{15}$$

where it is understood that the phase shift applied by the MZM is time dependent $\phi = \phi(t)$.

Since only one output of the MZM is used, we simply set the other output to zero at the coupler input

$$\mathbf{E}_{C1-in} = jE(t) \begin{bmatrix} \sin(\phi/2) \\ 0 \end{bmatrix}. \tag{16}$$

Assume the coupler is 50:50 and use the matrix in Fig. 2(a) to obtain

$$\mathbf{E}_{C1-out} = \frac{1}{\sqrt{2}} \begin{bmatrix} 1 & j \\ j & 1 \end{bmatrix} \left(jE(t) \begin{bmatrix} \sin(\phi/2) \\ 0 \end{bmatrix} \right) = \frac{jE(t)}{\sqrt{2}} \begin{bmatrix} \sin(\phi/2) \\ j\sin(\phi/2) \end{bmatrix}. \tag{17}$$

To account for differential time delay τ we employ the time-delay operator matrix of Fig. 2(d) to find, finally,

$$\begin{aligned} \mathbf{E}_q &= \begin{bmatrix} \Gamma(\tau) & 0 \\ 0 & 1 \end{bmatrix} \left(\frac{jE(t)}{\sqrt{2}} \begin{bmatrix} \sin(\phi/2) \\ j\sin(\phi/2) \end{bmatrix} \right) \\ &= \begin{bmatrix} (jE(t-\tau)/\sqrt{2})\sin(\phi(t-\tau)/2) \\ (-E(t)/\sqrt{2})\sin(\phi(t)/2) \end{bmatrix}. \end{aligned} \tag{18}$$

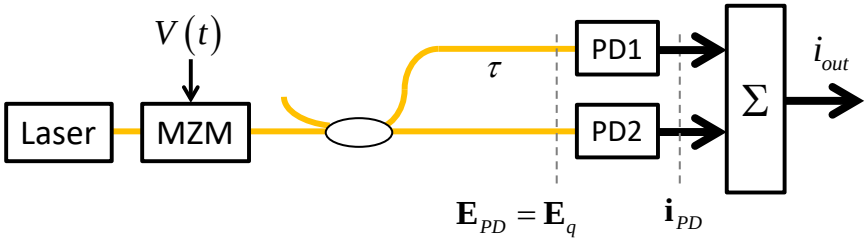

Figure 9: A 2-beam combination architecture in which the light in each path is individually photodetected and summed in the RF domain using a combining device Σ.

(Note: The subscript "q" has no special meaning here; we just needed a label to indicate this particular location in the partial system.) Equation (19) can be written succinctly as

$$\mathbf{E}_q = \frac{1}{\sqrt{2}} \begin{bmatrix} E_{M1}(t-\tau) \\ jE_{M1}(t) \end{bmatrix} \tag{19}$$

where E_{M1} denotes the MZM output field that is passed to coupler $C1$,

$$E_{M1} = \left(jE(t)/\sqrt{2} \right) \sin(\phi(t)/2). \tag{20}$$

We now proceed to the analyses and discussion of the approaches in Fig. 7.

4.1 Approach A: RF Combiner with Individual Photodetectors

The most straightforward approach is to simply photodetect the light in each fiber and combine the recovered RF signals in a multi-port RF combiner as shown in Fig. 7(A). Figure 9 shows a two-tap version where $\mathbf{E}_q$ was calculated above. The photocurrents at the two PD outputs will be represented here by a column vector $\mathbf{i}_{PD}$,

$$\mathbf{i}_{PD} = \begin{bmatrix} i_{PD1} \\ i_{PD2} \end{bmatrix} \propto \frac{1}{2} \begin{bmatrix} |E_{M1}(t-\tau)|^2 \\ |E_{M1}(t)|^2 \end{bmatrix}. \tag{21}$$

Defining $i_M(t) = (1/2)|E_{M1}(t)|^2$, the output of the RF summing device Σ is

$$i_{out} = i_{M1}(t-\tau) + i_{M1}(t) \tag{22}$$

which is the desired output for an FIR filter (cf Eq. (1)). Here $K = 1$ at the output of either photodetector since any photocurrent at PD1 must have come from photons traveling in the upper (delayed) arm, and similarly for PD2, so $\gamma^2 = 1 - K^2 = 0$ and this system cannot exhibit optical interference at the PD outputs. However, at the RF output i_{out}, we don't know the path taken by a signal in reaching that point so $K = 0$ and $\gamma = 1$ which indicates complete interference for RF signals is possible. Of course, this is desirable as it is exactly the principle by which an FIR filter works.

4.2 Approach B: Optical Combiner with a Single Photodetector

We next consider an approach in which the signals are combined in the optical domain using a fiber coupler as shown in Fig. 10 and the RF signal is obtained using a photodetector at one of the two coupler outputs. Starting with $\mathbf{E}_q$ from Eq.(19), the fields at the output of $C2$ are given by

$$\mathbf{E}_{C2-out} = \frac{1}{\sqrt{2}}\begin{bmatrix} 1 & j \\ j & 1 \end{bmatrix} \frac{1}{\sqrt{2}}\begin{bmatrix} E_{M1}(t-\tau) \\ jE_{M1}(t) \end{bmatrix} = \frac{1}{2}\begin{bmatrix} E_{M1}(t-\tau) - E_{M1}(t) \\ j\left(E_{M1}(t-\tau) + E_{M1}(t)\right) \end{bmatrix} \tag{23}$$

where, recall, $E_{M1}(t) = \left(jE(t)/\sqrt{2}\right)\sin(\phi(t)/2)$. Choose one of the coupler outputs to go to the PD,

$$E_{PD} = (1/2)\left(E_{M1}(t-\tau) - E_{M1}(t)\right). \tag{24}$$

Then the output photocurrent is

$$i_{out} \propto |E_{PD}|^2 = (1/2)\left[i_{M1}(t-\tau) + i_{M1}(t) - 2\gamma\Re e(E^*_{M1}(t-\tau)E_{M1}(t))\right] \tag{25}$$

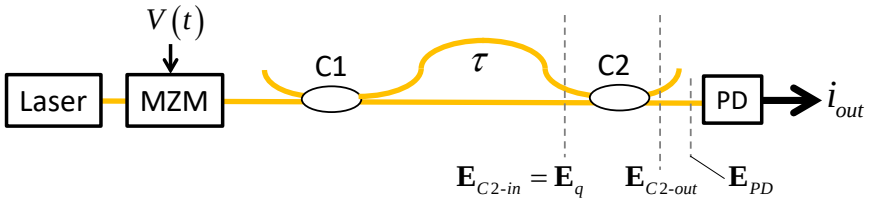

Figure 10: An all-optical 2-beam combination architecture in which the light in each path is summed in the optical domain using a fiber coupler and the RF is recovered by a photodetector at one of the two coupler outputs.

where $i_{M1}(t) \propto |E_{M1}(t)|^2$ and where $\Re e$ denotes the real part. The first two terms on the right side of Eq.(25) are good terms – they are the desired sum of photocurrents for a FIR filter. But the last term is bad – it represents optical interference and can produce instabilities in the RF output as the optical path difference between the two arms changes on a scale as small as fraction of an optical wavelength. If the optical interference is strong ($\gamma \approx 1$), and the path difference between the two arms is $\lambda/2$ where λ is the optical wavelength, then the output can fade to nearly zero, $i_{out} \to 0$. The filter disappears from this coupler output! But now all the light then exits the other coupler output fiber and the filter happily resides there. Note that if we photodetect both coupler outputs and perform the sum in the RF domain, coherent optical effects at the final RF output will indeed have been eliminated but, in doing so, we have inadvertently inserted a second RF interferometer in series with the first which will change the filter response function. One solution is to stabilize the optical interferometer either by active or passive techniques [Refs] but, of course, at an increase in system SWaP-C (size, weight, (and) power, and cost).

4.3 Approach C: Fiber Bundle with a Single Photodetector

In Approach A the summation of signals was performed in the RF domain and, in Approach B, the signals were combined in the optical domain. In Approach C, we perform the summation exactly at the interface between optical and RF domains, that is, directly on the surface of the photodetector where the fibers are first brought together into a bundle of a type described in the literature [15, 16, 17, 18]. We will refer to such a device as, simply, a fiber bundle (FB).

A two-tap version is shown in Fig. 11. Assuming no insertion loss, the

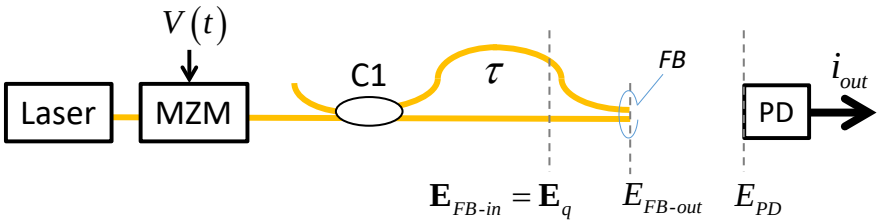

Figure 11: A 2-tap combination architecture using a fiber bundle (FB) to sum the signals directly at the interface between optical and electrical domains, that is, on the PD surface.

output is considered to be the same as the input $\mathbf{E}_{FB-out} = \mathbf{E}_q$ where E_q is given in Eq.(19). This is not exactly true because, although there is still some spatial separation between the signals at the FB output, there can also be significant overlap and interaction. More accurately, the output of the bundle should be treated as a so-called supermode but, thankfully, that distinction will be of no consequence once we analyze the total field at the PD.

Fundamentally, the fiber bundle operates as shown earlier in Fig. 4(a) where two or more light beams with different $\vec{k}$ vectors were superimposed onto a single PD. But, depending on the distance between the output of the FB and the PD surface, only partial summation of the signals may occur since some fraction of the light from the FB may never reach the PD.

Figure 12 shows details of the geometry of the FB-PD interface. Let $G_{a,b}(x, y)$ denote the complex, normalized spatial distribution of the E-field from fiber a and b, respectively, in the plane of the PD surface. We allow complex values because G may include optical phase information arising from the detailed structure of the supermode. In any case, we assume the G functions are normalized in power such that

$$\int_{-\infty}^{\infty}\int_{-\infty}^{\infty} |G_{a,b}(x,y)|^2 dxdy = 1. \tag{26}$$

With the geometry of the system defined by Fig. 12, the E-field at position (x, y) in the plane of the PD surface at time t is given by

$$\begin{aligned} E_(x,y,t) = \frac{1}{\sqrt{2}} [G_a(x,y) \exp(jkL_a) E_{M1}(t-\tau) \\ + jG_b(x,y) \exp(jkL_b) E_{M1}(t) \end{aligned} \tag{27}$$

where k is the magnitude of the optical wavevector, $k = 2\pi/\lambda$, λ is the optical wavelength, and L_a and L_b are the distances, respectively, between the output end of fibers a and b and the location (x, y) on the PD.

Now our goal was to construct an RF FIR filter and the time delay τ, therefore, is an RF time delay. If the filter is constructed properly, this delay should be stable. However, when the filter is implemented in the optical domain, there exists the potential danger of small, time-dependent variations lurking in the delay at optical length scales. These delay variations can give rise to optical phase shifts that will directly produce instabilities in the RF filter response whenever optical coherence effects are present. To account for this possibility we replace τ with

$$\tau \to \tau_0 + \Delta\tau(t). \tag{28}$$

where τ_0 is the stable, overall RF delay and $\Delta\tau(t)$ represents the small (optical scale), time-dependent variations in τ. We will assume the spectrum of variations in $\Delta\tau(t)$ lies predominantly at frequencies well below any RF frequency range of interest and well below $1/\tau$ and thus can be accounted for by a simple phase shift

$$E_{M1}(t-\tau) \rightarrow E_{M1}(t-\tau_0)\exp\left(j\delta(t)\right) \tag{29}$$

where $\delta(t) = 2\pi\nu\Delta\tau(t)$.

The optical power contained in a small area $dxdy$ of the plane containing the PD surface and centered at (x, y) (Fig.12) is

$$dp(x,y) \propto |E(x,y,t)|^2 dxdy \tag{30}$$

where

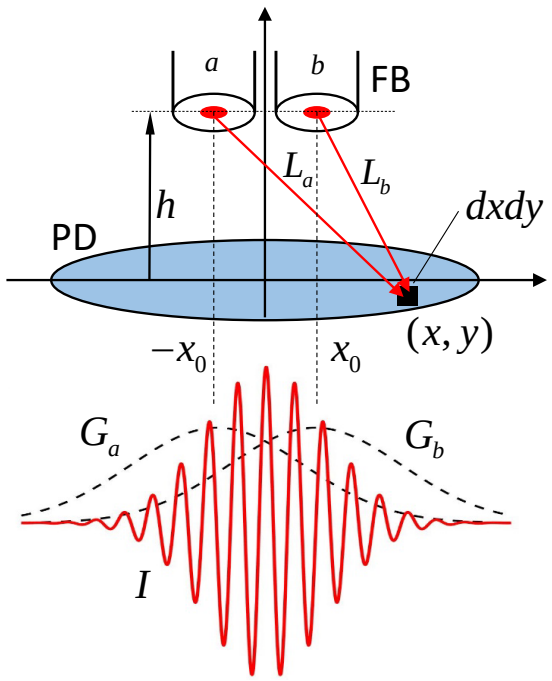

Figure 12: Geometry for analysis of a fiber bundle (FB) a distance h from the photodetector (PD) and assuming only two fibers a and b. Shown in red is an example interference pattern on the PD surface
$I = 2\Re e(G_a(x)G_b^*(x)\exp(jk\Delta L)$ for real-valued Gaussians G_a and G_b.

$$
\begin{aligned}
&|E(x,y,t)|^2 = \\
&\quad \frac{1}{2}\left[|G_a(x,y)E_{M1}(t-\tau)|^2 + |G_b(x,y)E_{M1}(t)|^2\right] \\
&\qquad + \Re e\left[G_a(x,y)G_b^*(x,y)\exp\left(jk\Delta L\right)\ldots\right. \\
&\qquad\quad \left.\ldots\ \exp\left(j\delta(t)E_{M1}(t-\tau_0)E_{M1}^*(t)\right)\right].
\end{aligned}
\tag{31}
$$

and where $\Delta L = (L_a - L_b)$.

The red curve at the bottom of Fig. 12 shows an example of the spatial interference pattern that can develop on the PD surface arising from the term

$$I_{int} = \Re e\left(G_a(x,y)G_b^*(x,y)\exp(jk\Delta L)\right). \tag{32}$$

To produce this curve we assumed the spatial distribution curves were both real-valued, Gaussian functions of one variable,

$$G_{a,b} = \frac{1}{\sqrt{2\pi\sigma^2}}\exp\left(\frac{-(x \mp x_0)^2}{2\sigma^2}\right) \tag{33}$$

where the $\mp$ sign corresponds to a and b, respectively, and where σ^2 is the variance of the distribution. These distributions are shown as the black, dashed curves in the figure. For the parameters h, x_0, and k we chose values simply to produce a realistic-looking interference pattern.

The total photocurrent is proportional to the integral of $dp(x,y)$

$$i_{out}(t) \propto \int\int_{PD\,surface} |E(x,y,t)|^2 dxdy. \tag{34}$$

where the integral is performed only over the PD surface. Hence, the output photocurrent comprises three terms

$$i_{out}(t) = i_a(t-\tau) + i_b(t) + i_c(t) \tag{35}$$

where

$$i_a(t-\tau) \propto \frac{1}{2}|E_{M1}(t-\tau)|^2 \int\int_{PD\,surface} |G_a(x,y)|^2 dxdy \tag{36}$$

$$i_b(t) \propto \frac{1}{2}|E_{M1}(t)|^2 \int\int_{PD\,surface} |G_b(x,y)|^2 dxdy, \tag{37}$$

and

$$i_c(t) \propto E_{M1}(t-\tau)E_{M1}^*(t) \int\int_{PD\,surface} |G_a(x,y)G_b^*(x,y)e^{jk\Delta L}|^2 dxdy. \tag{38}$$

The first two terms $i_a(t-\tau)+i_b(t)$ are exactly what we want for an FIR filter. Ideally, the last term – the interference term – should vanish and we now discuss the conditions under which that can occur.

If, instead of integrating just over the surface area of the PD in Eq. (38) we integrated from $-\infty$ to $+\infty$ in both directions, then the interference term is guaranteed to be zero. However, as Fig. 12 suggests, it is possible for some portion of the interference pattern to spill over the edge of the PD in which case i_c does not vanish in general. In addition, as $\delta(t)$ varies in time the entire interference pattern will shift position on the PD surface. This can be seen as follows. For the moment, assume that $\Delta L \approx (2x_0/h)x$. Then the exponential term in the integrand in Eq. (38) becomes

$$\exp\left(jk\Delta L\right)\exp\left(j\delta(t)\right) \rightarrow \exp\left(jk\left[\left(\frac{2x_0}{h}\right)x + c\Delta\tau\right]\right). \tag{39}$$

Thus small, time-dependent delay variations $\Delta\tau$ are equivalent to changes in x on the PD surface and the entire surface integral in Eq. (38) varies in time. That is, the entire interference pattern shifts unpredictably on the PD and locations on the perimeter of the PD are obviously affected most strongly. The net result is the appearance of temporal fluctuations in the filter function driven by small, optical-path fluctuations in the fibers that implement the filter.

In a sense, there are two different but related uncertainties at play here – one bad and one good. In the first, we are uncertain about whether any photon actually reached the PD and so, the certainty is given by

$$K^2 = (1-\gamma^2) = \frac{\int\int_{PD\,Surface}|E(x,y,t)|^2dxdy}{\int_{-\infty}^{\infty}\int_{-\infty}^{\infty}|E(x,y,t)|^2dxdy}. \tag{40}$$

$K \neq 1$ then gives rise to possible interferometric fluctuations. Secondly, once a photon does reach the PD, we don't know which delay path was taken but this uncertainty gives rise to the desired RF interference that produces the filter. Optical coherence effects are thus suppressed by engineering the device so the PD captures as much light that exits the TFB as possible.

4.4 Approach D: Multiplexing onto a Single Photodetector

In this section we analyze a few specific examples of the general approach shown in Fig. 7(D) where some type of optical splitting (DEMUX) and combining (MUX) technique are employed to first separate and then recombine the modulated signals onto a single optical fiber for subsequent

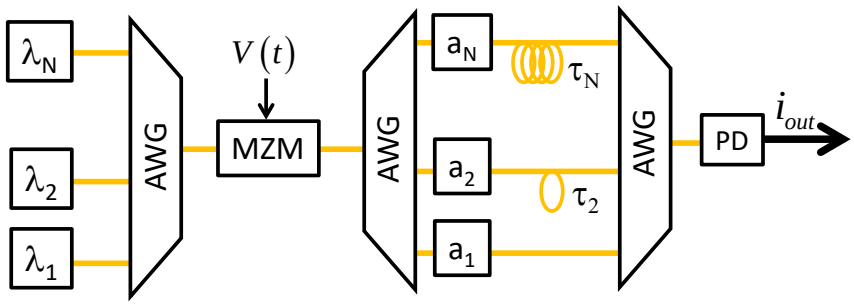

Figure 13: Application of WDM multiplexing technique for implementing an FIR fileter in the optical domain. AWG = arrayed-waveguide grating. a_n and τ_n denote the attenuation and delay, respectively, in the $n-$th delay line.

detection on a single photodetector. We examine three multiplexing techniques: i) wavelength-division multiplexing (WDM), ii) polarization-division multiplexing (PDM), and space-division multiplexing (SDM).

The WDM approach is ubiquitous in modern fiber digital communications systems; the PDM approach, also used extensively in high-speed digital fiber communication systems, is probably the easiest of the three MUX approaches to implement in terms of hardware and system design; and, finally, SDM is a relatively new approach and will be discussed only briefly.

4.4.1 Wavelength-Division Multiplexing

A possible WDM architecture for an optical-domain FIR filter is shown in Fig. 13 in which the light from N lasers, each operating at a different wavelength λ_n, is combined onto a single fiber at the input to an MZM using an arrayed-waveguide grating (AWG). The light at all wavelengths is then modulated by one MZM with its output connected to a second AWG which puts the light at each wavelength back onto separate fibers to allow individual attenuations and delays to be applied. A third AWG recombines all the signals back onto one fiber for photodetection. Implementation issues in this case are the SWaP-C associated with multiple lasers and the three AWGs.

4.4.2 Polarization-Division Multiplexing

A straightforward multiplexing approach to optical-domain FIR filters is polarization-division multiplexing (PDM). (Note: Some authors use "PM"

to denote polarization multiplexing but be aware that PM is also used frequently to denote polarization-maintaining (optical fiber)). Figure 14(a) shows an architecture for implementing a two-tap FIR filter using PDM that will be used for analysis, and Fig. 14(b) shows a generic multi-tap version. Polarization-maintaining (PM) fiber, shown in blue in the figure, is used throughout the system.

At this point a quick review of polarization states and bases may be helpful. And this brings us to the one exception alluded to in the Introduction in which we noted that a scalar description of the E-field may not be sufficient for system analysis. Importantly, the matrices summarized in Fig. 2 *do not* apply to Jones vectors and thus cannot be used directly to analyze this system.

Recall that light is a vector field and is thus described in space by a three-component vector. In vacuum and, to a good approximation in fiber, the E-field vector is always transverse to the direction of propagation and can thus be described entirely by just a two-component vector, sometimes called a Jones vector, which completely specifies the state of polarization

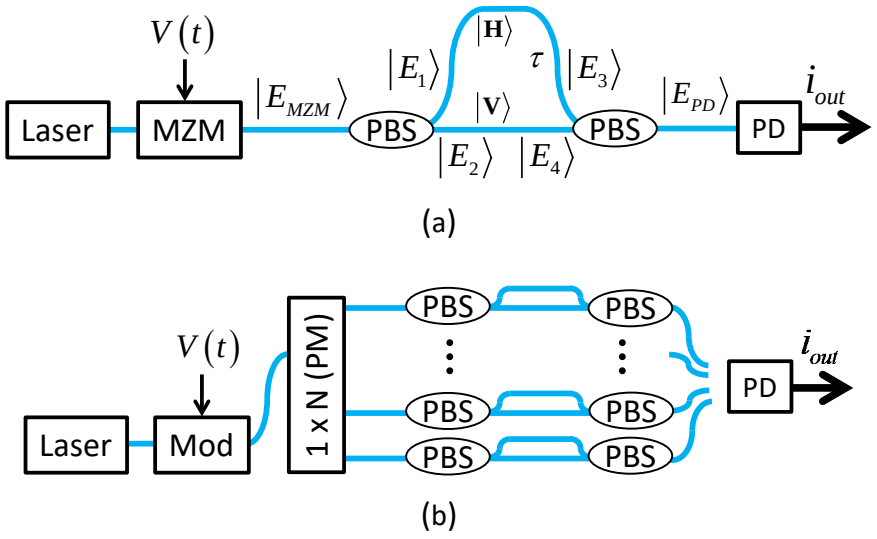

Figure 14: (a) A two-tap polarization-multiplexing system where $|H\rangle, |V\rangle$ indicate horizontal and vertical polarization states, respectively and the Jones states $|E_n\rangle$ are indicated at various locations in the system. PBS = polarizing beam splitter. (b) A generic multi-tap polarization-multiplexing approach to implementing a FIR filter. Polarization-maintaining (PM) fiber, shown in blue, is used throughout.

(SOP) of the light. Like any 2-dimensional vector, any Jones vector can be expressed with respect to a basis comprising a set of two orthonormal basis vectors or, in this case, two orthonormal polarization states. The most common choice of basis set are the horizontal and vertical SOPs that we will denote as $|H\rangle$ and $|V\rangle$, respectively. In their own basis,

$$|H\rangle = \begin{bmatrix} 1 \\ 0 \end{bmatrix} \quad \text{and} \quad |V\rangle = \begin{bmatrix} 0 \\ 1 \end{bmatrix}. \tag{41}$$

Any Jones vector $|E\rangle$ can be written as a linear combination $|E\rangle = \alpha\,|H\rangle + \beta\,|V\rangle$ where the weighting coefficients α and β are complex in general. To calculate optical power we need to determine the magnitude-squared of the field. In the case of a scalar field we calculate, simply, $|E|^2 = E \cdot E^*$. For Jones vectors we instead must use the inner product

$$|E|^2 = \langle E|E\rangle = \left(\langle H|\,\alpha^* + \langle V|\,\beta^*\right)\left(\alpha\,|H\rangle + \beta\,|V\rangle\right) \tag{42}$$

where

$$\langle H| = \begin{bmatrix} 1 & 0 \end{bmatrix} \quad \textit{and} \quad \langle V| = \begin{bmatrix} 0 & 1 \end{bmatrix}. \tag{43}$$

To complete the story, there are many optical systems in which the performance is insensitive to the SOP of the input light so, in analyzing such systems, there is no need to keep track of both polarization components. Here can keep track of just one component, that is, just a scalar field and this was the case for all the previous analyses in this report.

The fundamental element in any PDM system is the so-called polarizing beam splitter (PBS) which, when used in the reverse direction, becomes a polarizing beam combiner. We will use simply "PBS" in both cases. When used as a beam splitter, a PBS takes the portion of input light that is horizontally polarized and directs it to one output, say, the upper output as shown in Fig. 14(b) and directs any vertically-polarized light at the input to the other output. Each polarization component is then individually attenuated and delayed before recombination onto one fiber prior to photodetection using a second PBS .

We now analyze the 2-tap system in Fig. 14(a). Suppose the output of the MZM is in a linear SOP oriented at 45 deg to the $|H\rangle$ and $|V\rangle$ states of the first PBS,

$$|E_{MZM}\rangle = \frac{E(t)}{\sqrt{2}}\begin{bmatrix} 1 \\ 1 \end{bmatrix} = \frac{E(t)}{\sqrt{2}}\,|H\rangle + \frac{E(t)}{\sqrt{2}}\,|V\rangle. \tag{44}$$

With the fields labelled as shown in Fig. 14(a), we have

$$|E_3\rangle = \frac{E(t-\tau)}{\sqrt{2}}\,|H\rangle \quad \text{and} \quad |E_4\rangle = \frac{E(t)}{\sqrt{2}}\,|V\rangle \tag{45}$$

so

$$|E_{PD}\rangle = \frac{E(t-\tau)}{\sqrt{2}}|H\rangle + \frac{E(t)}{\sqrt{2}}|V\rangle . \tag{46}$$

The optical power is proportional to

$$\begin{aligned} |E_{PD}|^2 &= \langle E_{PD}|E_{PD}\rangle \\ &= \frac{1}{2}\left(|E(t-\tau|^2 + |E(t)|^2 + E^*(t-\tau)E(t)\langle H|V\rangle + \right. \\ &\qquad \left. E(t-\tau)E^*(t)\langle V|H\rangle\right) \end{aligned} \tag{47}$$

where we used $\langle H|H\rangle = \langle V|V\rangle = 1$. It is clear that the two interference terms vanish in this case due to the orthogonality of $|H\rangle$ and $|V\rangle$, that is, $\langle H|V\rangle = \langle V|H\rangle = 0$. It is also clear that interference may occur if the two fields incident on the PD are not exactly orthogonal which can arise from non-ideal operation of the PBSs or from improper splices between different segments of PM fiber.

Figure 14(b) shows a possible extension of the 2-tap architecture to a multi-tap architecture. Here, a $1 \times N$ PM splitter provides the inputs to N individual PBS splitter devices which then each provide two distinct delay lines. Once the two beams combine and reach the output of the second PBS we are effectively back at the situation faced by the systems of Figs. 7(A), (B), and (C).

4.4.3 Space-Division Multiplexing

In this last subsection on multiplexing, we discuss only qualitatively a few relatively new approaches that depend on the use of custom-designed fibers. Currently, these techniques are not in wide-spread use and it remains to be seen whether they ever will. The approaches fall under the general heading of space-division multiplexing (SDM) that refers, generally, to a multiplexing technique that establishes "... multiple, independent data paths through a single optical fiber."[19]. Notice the words "single optical fiber" and not singlemode optical fiber. SDM fibers are highly-customized waveguide structures designed to achieve low transmission loss, low crosstalk, and ease of independent addressability for some choice of spatial mode family. The custom fibers come in three design types that can be sorted into two broad categories. In the first category, a single fiber contains multiple cores that are spatially separated (Fig. 15(a)) to such an extent that crosstalk between cores is low. This fiber thus acts as a single structure containing N independent, singlemode waveguides. In the second broad category the waveguides

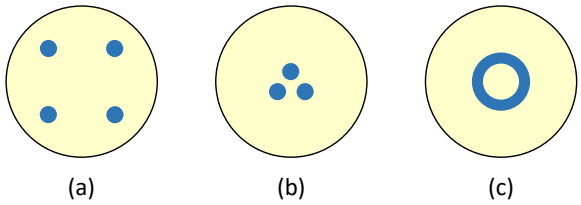

Figure 15: Three common core configurations for SDM shown schematically. (a) Cores well separated to carry multiple, independent, single modes. (b) Cores close enough together to support multiple supermodes. (c) Ring core to support multiple OAM modes.

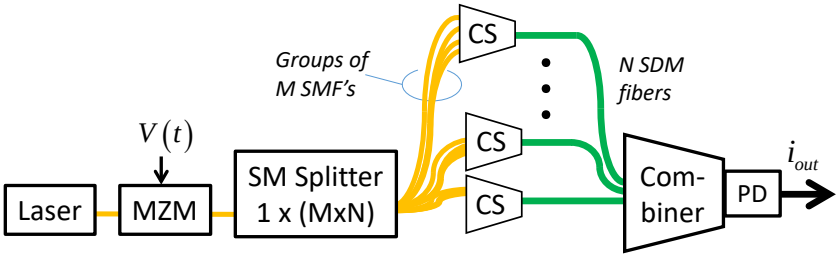

Figure 16: A conceptual design for utilizing space-division multiplexing (SDM) to implement an FIR filter having $M \cdot N$ taps. CS = coupling structure to inject the output of each SM fiber into a particular mode of the corresponding SDM fiber (shown in green)

.

are designed to support what is sometime called mode-division multiplexing (MDM). As the name suggest, in this approach independent signals are carried on different, often overlapping modes. MDM itself comprises two general approaches: i) supermodes, and ii) orbital angular momentum (OAM) modes. In the supermode approach, the individual cores are brought close enough together (Fig. 15(b)) so that all the cores "talk" to one another. The result is a waveguide that supports a number of so-called supermodes, typically 6-10 in number, for a single fiber. In the OAM approach, the fiber employs a ring core as shown in Fig. 15(c) to match the donut shape of the OAM modes. The SDM fibers that are available commercially today typically have some means to address each core or each supermode in the fiber individually. Figure 16 shows a conceptual SDM design for a multiple-tap FIR filter. In the figure, we refer to the device that accomplishes coupling

from an individual standard, singlemode fibers to an individual path in a single, custom SDM fiber as, simply, a "coupling structure" (CS).

5 Parallel versus Serial Implementations

Before concluding this report we wish to address briefly the following issue. In the entire discussion up to now we have assumed that the optical-domain implementation of the FIR filter employed a parallel array of N delay lines (Fig. 17(a)). But it is also possible to implement a filter using a serial arrangements of pairs of delay lines as shown in Fig. 17(b), an architecture that is also referred to as a generalized lattice filter and, for a specific choice of delays, as a Fourier filter [4].

In this section we will discuss briefly some of the trade-offs between the two architectures and also answer the question of whether there is a one-to-one correspondence between the two approaches. That is, given a parallel FIR with filter function specified by delays $(\tau_1, \tau_2, \cdots, \tau_N)$, is it always possible to construct a serial FIR with delays $(T_1, T_2, \cdots, T_N)$ the same filter function? And vice-versa? These questions are not unique to optical-domain implementations, of course, but we raise the issue here for

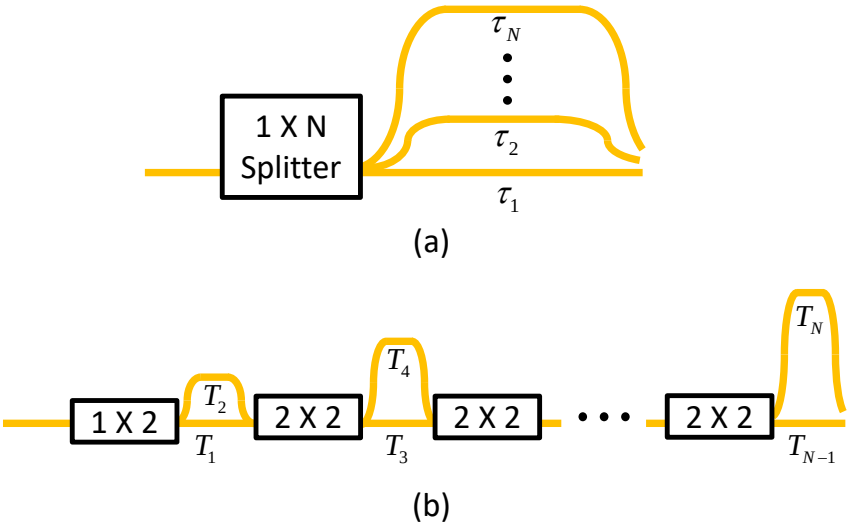

Figure 17: Optical domain implementations of an FIR filter using (a) a parallel array of N delay lines, and (b) a series array of delay lines.

reasons that will become apparent shortly.

If we start with a filter implemented serially then the answer is yes, a parallel filter can always be implemented that has exactly the same filter function by simply choosing the same delays and weightings. Note that this is *not* the simple correspondence $\tau_n = T_n$ since, for example, the smallest overall delay in the serial structure is the sum of all the shorter delays in each $2x2$ sub-assembly. Instead, we would choose $\tau_1 = T_1 + T_3 + T_5 + \cdots + T_{N-1}$, $\tau_2 = T_2 + T_3 + T_5 + \cdots + T_{N-1}$ and so on. Going the other direction, that is, implementing a specific parallel FIR in the form of a serial structure, is not generally possible. We see immediately that the number of taps in the serial array must be a power of two, $N = 2^m$, where m is the number of couplers. Hence, a parallel filter for which the number of taps $N \neq 2^m$ for some integer m cannot be implemented serially. But even if the number of taps in the original parallel filter was a power of two, an equivalent serial implementation is not generally possible.

As an example, suppose we are given the specifications for a 4-tap, parallel FIR filter, namely, $(\tau_1, \tau_2, \tau_3, \tau_4)$ and (a_1, a_2, a_3, a_4). There are only four distinct delays in the serial filter which must be set equal to the four delays in the parallel filter,

$$\begin{cases} T_1 + T_3 = \tau_1 \\ T_2 + T_3 = \tau_2 \\ T_1 + T_4 = \tau_3 \\ T_2 + T_4 = \tau_4. \end{cases} \tag{48}$$

We thus need to solve for the four T_n values satisfying these four linear equations in four unknowns,

$$\begin{bmatrix} 1 & 0 & 1 & 0 \\ 0 & 1 & 1 & 0 \\ 1 & 0 & 0 & 1 \\ 0 & 1 & 0 & 1 \end{bmatrix} \begin{bmatrix} T_1 \\ T_2 \\ T_3 \\ T_4 \end{bmatrix} = \begin{bmatrix} \tau_1 \\ \tau_2 \\ \tau_3 \\ \tau_4 \end{bmatrix}. \tag{49}$$

Unfortunately the determinant of this 4×4 matrix is zero and, hence, this set of equations cannot be solved.

However, from a practical standpoint 2×2 couplers are much easier to acquire and use than $N \times N$ couplers, especially for $N \geq 4$. In addition, with the serial implementation, the final combiner must deal with only 2 fibers, even for N taps. And it should be noted that all the possible coherent optical effects discussed earlier are still present in the serial architecture. But if the appropriate optical-domain filter can be designed and implemented serially, there may be significant practical advantages for that approach.

6 Summary

We have investigated theoretically four approaches for implementing a parallel, finite-impulse-response (FIR) filter in the optical domain. We showed that a significant challenge to implementation was finding a method for combining the multiple, time-delayed optical signals to produce a single RF output having the proper filter characteristics. Our main goal was to understand and quantify possible deleterious effects on filter performance arising from optical coherence.

To this end, it is always necessary to determine the total optical field at the photodetector and then calculate the output photocurrent. We provided a set of matrices representing various system elements that streamlined calculation of the optical E-fields as they propagated through the system. Optical interference effects make their appearance as unwanted terms in the output photocurrent.

We discussed briefly the origins of optical interference and proposed that thinking about interference in terms of uncertainty could be more powerful than thinking in terms, simply, of overlap of signals.

We analyzed four different optical-domain FIR filter configurations. In each case we calculated the contribution of optical interference on the filter output and discussed ways to mitigate the optical interference while maintaining the RF interference necessary for filter operation.

Finally, we discussed briefly the correspondence between optical-domain FIR filters implemented using a parallel array of fibers and those employing a serial array of fibers.

References

[1] J.D. McKinney V.J. Urick Jr. and K.J. Williams. Fundamentals of Microwave Photonics. Wiley, 2015.

[2] W.S.C. Chang. RF Photonic Technology in Optical Fiber Links. Cambridge, 2002.

[3] III C.H. Cox. Analog Optical Links. Cambridge, 2004.

[4] C.K. Madsen and J.H. Zhao. Optical Filter Design and Analysis. Wiley, 1999.

[5] D.M. Pozar. Microwave Engineering. Wiley, 2005.

[6] F.L. Pedrotti Sr. and L.S. Pedrotti. Introduction to Optics. Prentice Hall, 1993.

[7] W. H. Steel. Interferometry. Cambridge, 1983.

[8] M. Francon. Optical Interferometry. Academic Press, 1966.

[9] *The double slit experiment*. 2019. URL: `https://physicsdetective.com/the-double-slit-experiment/`.

[10] *Optics basics: Young's double slit experiment*. 2009. URL: `https://skullsinthestars.com/2009/03/28/optics-basics-youngs-double-slit-experiment`.

[11] P. Storey, S. Tan, M. Collett and D. Walls. "Path detection and the uncertainty principle ". *Nature* 367(17) (1994), pp. 626–628.

[12] Y.-H. Kim, R. Yu, S.P. Kulik, Y. Shih and M.O. Scully. "Delayed "choice"quantum eraser ". *Phys. Rev. Lett.* 84(1) (2000), pp. 1–5.

[13] A. Ananthaswamy. Through Two Doors at Once. Dutton, 2019.

[14] B.-G. Englert. "Fringe visibility and which-way information: An inequality". *Phys. Rev. Lett.* **77**(11) (1996), pp. 2154–2157.

[15] S.G. Leon-Saval, T.A. Birks, J. Bland-Hawthorn, and M. Englund. "Multimode fiber devices with single-mode performance ". *Opt. Lett* 30(19) (2005), pp. 2545–2547.

[16] D. Noordegraaf, P.M.W. Skovgaard, M.D. Nielsen, and J. Bland-Hawthorn. "Efficient multi-mode to single-mode coupling in a photonic lantern ". *Opt. Exp.* 17(3) (2009), pp. 1988–1994.

[17] S. Yerolatsitis, I. Gris-Sánchez and T. A. Birks. "Adiabatically-tapered fiber mode multiplexers ". *Opt. Exp.* 22(1) (2014), pp. 608–617.

[18] T.A. Birks, I. Gris-Sánchez, S. Yerolatsitis, S.G. Leon-Saval and R.R. Thomson. "The photonic lantern ". *Adv. Opt. Photonics* 7(2) (2015), pp. 107–167.

[19] D.J. Richardson, J.M. Fini and L.E. Nelson. "Space-division multiplexing in optical fibres". *Nature Phot.* 7 (2003), pp. 354–362.